Simulation of laser-induced rectification in a nano-scale diode

Daniel Kidd,[1] Xiaojia Xu,[1] Cody Covington,[1] Kazuyuki Watanabe,[2] and Kálmán Varga[1,a)]
[1]Department of Physics and Astronomy, Vanderbilt University, Nashville, Tennessee 37235, USA
[2]Department of Physics, Tokyo University of Science, Shinjuku, Tokyo 162-8601, Japan

(Received 12 December 2017; accepted 17 January 2018; published online 6 February 2018)

Time-dependent density functional theory is utilized to simulate an asymmetrical jellium model, representing a nano-scale vacuum-tube diode comprised of bulk lithium. A sharp tip on one end of the jellium model allows for enhanced field emission upon interaction with an external laser field, leading to a preferential net current direction. This is verified by comparing the rate of electron transfer between the effective anode and cathode tips for both the diode jellium model and a symmetric cylinder jellium shape for various laser phase parameters. This rate of transfer is shown to significantly increase with smaller separation distances. With stronger laser intensities, this rate similarly increases but levels off as local near-field enhancements become negligible. *Published by AIP Publishing.*
https://doi.org/10.1063/1.5019259

I. INTRODUCTION

The modern age of electronics was marked by the development of the integrated circuit whose foundation was the semiconductor-based transistor. This technology allowed for low power consumption, reliability, and intuitive circuit design, thereby outpacing and replacing the earlier relied upon vacuum-tube-based implements. Such semiconductor-based devices have been the backdrop of the advancing field of electronics for many years; however, as the push for ultrafast operating speeds approaches the petahertz range,[1] the limited electron transport velocity of semiconductor transistors presents a formidable obstacle. Recent interest in electron photo-emission from metal nanotips,[2–5] motivated by improved ultrafast laser-guidance of electrons,[6–13] has inspired research pointing back in the direction of vacuum transport as a path towards achieving such higher speeds, with some prototype transistor devices being fabricated in the last few years.[14–17]

In this study, we focus on the template of Higuchi *et al.*[17] who take advantage of asymmetric near-field enhancement of two facing tungsten tips in order to achieve laser-driven rectification. It was found that by inducing electron emission from either tip using a few-cycle laser pulse, a sharper tip may act as an anode and an opposite dull tip may act as a cathode due to the relative emission rates which allow for an effective one-way total current. Because of the short duration of the multi-photon photoemission process, the high kinetic energy of the emitted electrons, and the sub-micron separation distance between the opposing tips, it was claimed that this device was able to operate on the sub-picosecond time scale. Furthermore, it was noted that faster electron transport may be possible for smaller separation distances due to stronger field enhancement and, in the sub-nanometer separation regime, prominent tunneling channels.[18]

This investigation of laser-driven nano-scale rectification is pursued by means of simulation via real-time time-dependent density functional theory (RT-TDDFT) applied to a jellium model of a lithium cluster. We employ the local density approximation (LDA) which has been shown, in conjuncture with jellium models, to yield results which will resemble the description of electronic excitations in bulk metal counterparts.[19–23] In this paper, we choose a jellium shape which models facing sharp and flat tips and excite the system with a homogeneous laser field in order to simulate an induced preferential net current direction. This effect is verified by comparing transfer rates to those of a geometrically symmetric jellium system—effectively two facing flat tips. We show that for small separation distances between sharp and flat tips, the magnitude of the preferential current significantly increases. Furthermore, we show that this current similarly increases for strong laser intensities; however, as local near-field enhancements become less significant, electron emission rates from either tip become more similar, resulting in a leveling off of the electron transfer rate.

II. MODEL

The shape of our lithium jellium model is that of a cylinder with one end capped by a cone—see Fig. 1. Periodic boundary conditions are enforced so that electron density leaving from either end of the jellium model travels between the two sites by wrapping through the boundary of the computational box, a process analogous to the facing tips of Higuchi *et al.* The system of study in this work, then, is truly an infinitely repeating chain of pointed jellium diode devices. It is worth noting that similar asymmetric structures have been studied within graphene nanoribbons and shown to produce rectification effects in areas such as electron transport across junctions[24] and thermal conductivity.[25]

The sharp tip of the jellium is expected to induce field enhancement[26,27] which, in turn, is expected to result in amplified electron emission at that site. The directionally favored electron emission is expected to lead to a preferential net current direction traveling in the direction of sharp tip to flat tip. The flux is to be measured at the midpoint between the two tips and then integrated with respect to time in order to determine the effective rate of electron density

a)kalman.varga@vanderbilt.edu

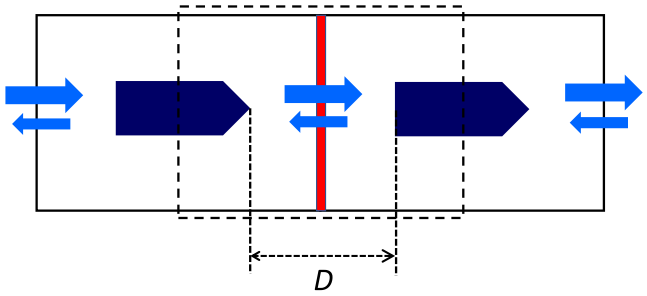

FIG. 1. Schematic of two neighboring cells within the model system, presented as a two-dimensional slice through the middle. The jellium diode shape (dark blue) is centered within a periodic computational box of width 27 Å in directions perpendicular to the axis of symmetry. The length of the box is adjusted in order to vary the effective separation distance, D, between the sharp and flat ends of the diode shape. The sharp cone tip experiences enhanced field emission (light blue), resulting in a preferential current in the direction of sharp end to flat end (left to right in this schematic). The flux is measured at the midpoint between the two tips (red), which is essentially either the left or right boundary of the box. The dashed line box indicates the similarity of this model to the facing nano-scale tips of Higuchi *et al.*[17]

transfer. The cylindrical portion of the jellium is given a radius of 3.43 Å, with the angle of the cone-shape cap as 80°. The total length of the shape is then 20 Å, in order to yield a volume corresponding to a cluster of 30 lithium atoms. The length of the box may be adjusted in order to vary the separation distance between the tips. We note that while lattice vibrations are neglected in this model, the time scale of the present simulations is shorter than that of such dynamics. Furthermore, the effect of temperature on this system is expected to play an insignificant role compared to the strong laser field strengths used.

III. FORMALISM

In RT-TDDFT, one describes the evolution of the electron density, $\rho(\mathbf{r},t)$, by solving the time-dependent Kohn–Sham equation

$$i\hbar\frac{\partial\phi_j(\mathbf{r},t)}{\partial t}=\left[-\frac{\hbar^2}{2m}\nabla^2+V_{\mathrm{KS}}[\rho](\mathbf{r},t)\right]\phi_j(\mathbf{r},t), \quad (1)$$

in order to obtain the time-dependent Kohn–Sham orbitals, $\phi_j(\mathbf{r},t)$. The density may then be determined as

$$\rho(\mathbf{r},t)=2\sum_{j=1}^{N}|\phi_j(\mathbf{r},t)|^2, \quad (2)$$

where N represents the total number of orbitals employed. The Kohn–Sham potential, $V_{\mathrm{KS}}[\rho]$, is a functional of the density and consists of three terms: (1) the Hartree potential

$$V_{\mathrm{H}}(\mathbf{r},t)=\frac{1}{4\pi\epsilon_0}\int\frac{\rho(\mathbf{r}',t)}{|\mathbf{r}-\mathbf{r}'|}d\mathbf{r}', \quad (3)$$

which governs the approximate electron-electron Coulomb interaction, (2) the exchange-correlation potential, for which we are using the LDA, and (3) the external potential, V_{ext}, which corresponds to all other interactions. In this work, the Hartree potential is determined at each time step by solving the Poisson equation via fast Fourier transforms. We note that the LDA model for the exchange-correlation potential does not take into account discontinuities that arise as a function of time and space[28–30] and influence transport dynamics such as tunneling rates in molecular junctions and ionization rates in molecules. While the LDA functional provides qualitatively correct results, a more sophisticated functional might be capable of returning quantitatively accurate transfer rates for more realistic model systems.

In this simulation, the external potential consists of two interactions

$$V_{\mathrm{ext}}=V_{\mathrm{bg}}+V_{\mathrm{laser}}. \quad (4)$$

The first is with respect to the static, positive background density

$$V_{\mathrm{bg}}(\mathbf{r})=\frac{-1}{4\pi\epsilon_0}\int\frac{\rho_{\mathrm{bg}}(\mathbf{r}')}{|\mathbf{r}-\mathbf{r}'|}d\mathbf{r}'. \quad (5)$$

Here, $\rho_{\mathrm{bg}}(\mathbf{r})$ is homogeneous within the boundary of the chosen jellium model shape, where the value is determined using the density parameter $r_s=1.72$ Å, corresponding to bulk lithium. The second is that of the external laser field, which is represented by its associated vector potential $\mathbf{A}(t)$

$$V_{\mathrm{laser}}(\mathbf{r},t)=\frac{1}{2m}|\mathbf{A}(t)|^2-\frac{i\hbar}{m}\mathbf{A}(t)\cdot\nabla. \quad (6)$$

This representation is known as velocity gauge and is most commonly expressed in combination with the kinetic term in Eq. (1) in order to concisely write a modified kinetic energy term

$$T(\mathbf{r},t)=\frac{1}{2m}[-i\hbar\nabla+\mathbf{A}(t)]^2. \quad (7)$$

The form of the laser field used is a variation of the smooth turn-on pulse[31]

$$\mathbf{E}_{\mathrm{laser}}(t)=\begin{cases}-\mathbf{E}_0\sin\left(\frac{\pi t}{2T_{\mathrm{r}}}\right)\sin(\omega t+\varphi), & \text{if } 0\le t\le T_{\mathrm{r}},\\ -\mathbf{E}_0\sin(\omega t+\varphi), & \text{otherwise,}\end{cases} \quad (8)$$

where T_{r} is the ramping time and φ is the phase of the laser. The vector potential is then determined as

$$\mathbf{A}(t)=-\int_0^t\mathbf{E}_{\mathrm{laser}}(t')dt'. \quad (9)$$

The Volkov state basis representation is used to describe and time propagate the Kohn–Sham orbitals.[32,33] This propagation technique is best suited for describing interactions with intense laser fields and allows for greater computational speeds than other conventional propagation methods. The states used to describe the system at $t=0$ correspond to the Fourier transform of a real-space grid with a grid spacing of 0.25 Å in each direction.

IV. RESULTS

The jellium model system was subjected to a laser of wavelength 780 nm, polarized parallel to the axis of symmetry,

which induced an oscillating current in the computational box. This current,

$$\mathbf{j}(\mathbf{r},t) = 2\sum_{j=1}^{N}\frac{\hbar}{2mi}(\phi_j^*\nabla\phi_j - \phi_j\nabla\phi_j^*) + \frac{1}{m}\mathbf{A}\rho, \tag{10}$$

was used to define the resulting flux, determined at the location of the plane bisecting the two edges of the jellium model, z_0, as

$$\Phi(z_0,t) = \int \mathbf{j}(\mathbf{r},t)\delta(z-z_0)d\mathbf{r} \tag{11}$$

which was integrated over time in order to ascertain the probability density transfered, N_{tr}

$$N_{\mathrm{tr}}(t) = \int_0^t \Phi(t')dt'. \tag{12}$$

Figure 2 shows this result for an example scenario of a separation distance, D, of 30 Å, a field intensity, I, of 1.33×10^{13} W/cm^2, and a short field ramping time of $T_{\mathrm{r}} = 2.48$ fs. Here, positive values for N_{tr} relate to a transfer of probability density from sharp to flat edges of the jellium model, i.e., left to right with respect to the schematic in Fig. 1. In each simulation, the small time regime ($t \leq 15$ fs) was well described by a linear trending sine curve. This section was fit by means of linear regression and the probability density transfer rate, k_{tr}, was determined as the slope of the resulting trend line. The rate of transfer tended to level off soon after this region in each simulation. This is most likely due to the increasing amount of high-energy orbitals being ionized from the jellium and following the field as nearly free particles. In this way, the near-field enhancement becomes more negligible to the physics described within the computational box as the simulation progresses.

The laser phase dependence of the transfer rate is shown in Fig. 3 for parameters $D = 30$ Å and $I = 1.33 \times 10^{13}$ W/cm^2. A symmetrically shaped cylinder without a cone cap was substituted in Fig. 3(a) in order to serve as a control test

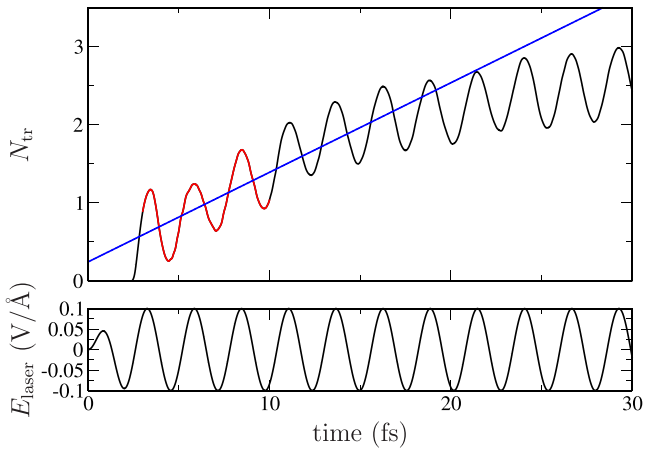

FIG. 2. Probability density transferred through the plane bisecting the two jellium model edges (top) for the example case of $D = 30$ Å, using a laser field of $I = 1.33 \times 10^{13}$ W/cm^2 and $T_{\mathrm{r}} = 2.48$ fs (bottom). A linear fit (blue) was fit by linear regression applied to the data sampled between $t = 3$ and $t = 10$ fs (red).

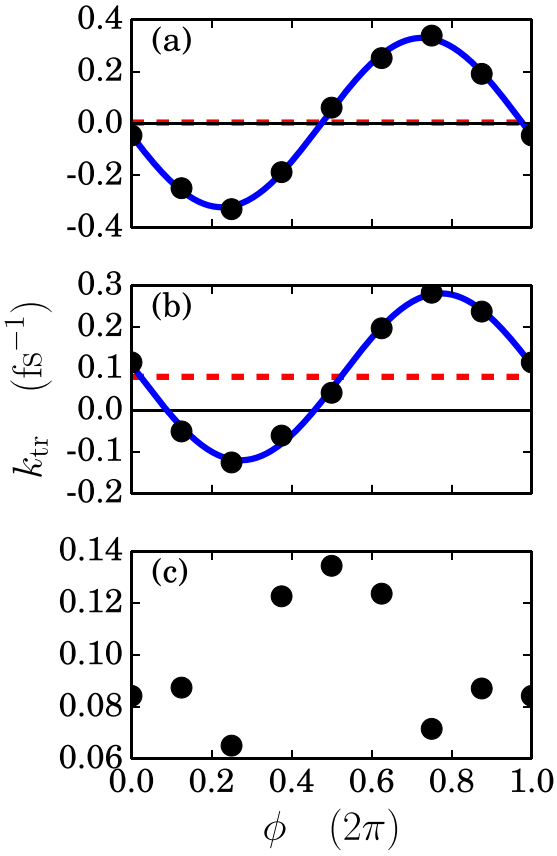

FIG. 3. Phase dependence of the probability density transfer rate for (a) a symmetric jellium cylinder shape without a cone cap and with a ramping time of $T_{\mathrm{r}} = 2.48$ fs, (b) the diode jellium model with a ramping time of $T_{\mathrm{r}} = 2.48$ fs, and (c) the diode jellium model with a ramping time of $T_{\mathrm{r}} = 9.94$ fs. For results using the shorter ramping time, a sinusoidal fit (blue line) shifted by an offset along the y-axis (dashed red line) was determined via linear regression. Each simulation employed parameters $D = 30$ Å and $I = 1.33 \times 10^{13}$ W/cm^2.

under geometrically symmetric conditions. In this case, while the shape of the jellium is symmetric, the phase, in combination with the short ramp time, provides a source of asymmetry by significantly lowering the effective potential barrier on one end of the jellium before the other. This causes a preferred current direction in the early time steps of the simulation. The trend observed is well described as a sine curve, whose vertical shift only varies from the zero axis by 0.004 fs^{-1} (1% of the amplitude). This insignificant offset indicates that no particular direction along the axis of symmetry is favored when the influence of the phase is neglected. However, for the case of the diode shape, Fig. 3(b), the same trend may be applied with an offset of 0.080 fs^{-1} (40% of the amplitude), indicating a preferential current in the direction of sharp to flat edges. A longer ramping time of $T_{\mathrm{r}} = 9.94$ fs was also employed using the diode shape, Fig. 3(c), in order to demonstrate positive transfer rates for any choice of phase. In this case, no such discernible trend was determined.

The dependence of the transfer rate on the separation distance is presented in Fig. 4. For each value of D, two simulations were performed using a phase of either 0 or π. The two results for k_{tr} were then averaged together in order to eliminate the phase dependence. Even for the smallest separation distance of 20 Å, the potential barrier is wide enough as to not

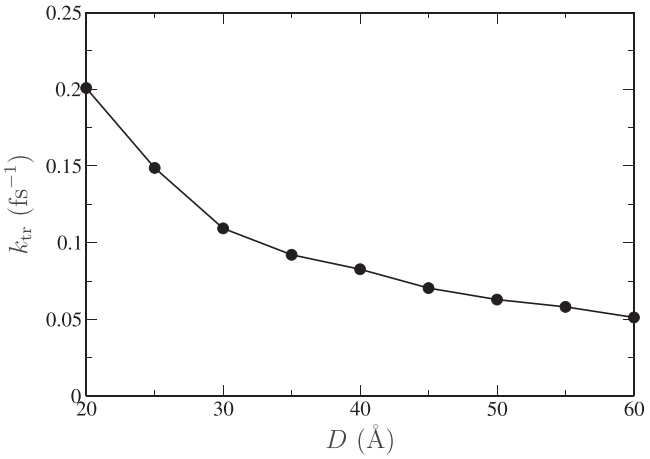

FIG. 4. Separation distance dependence of the probability density transfer rate for the jellium diode shape using a ramping time of $T_{\rm r} = 9.94$ fs and an intensity of $I = 1.33 \times 10^{13}$ W/cm^2. Data points have been connected with a solid line in order to guide the eye.

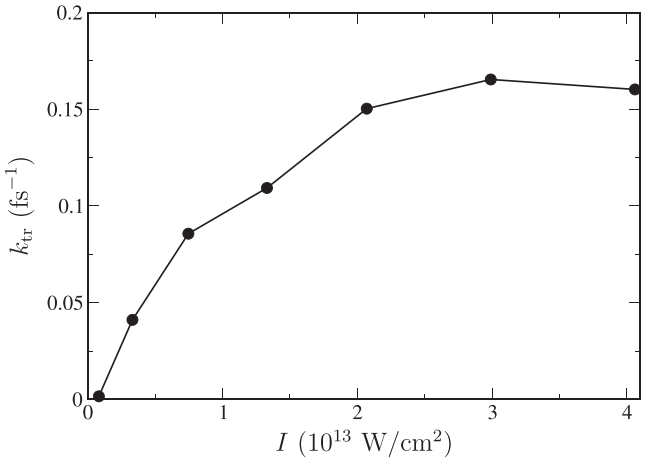

FIG. 6. Intensity dependence of the probability density transfer rate for the jellium diode shape using a ramping time of $T_{\rm r} = 9.94$ fs and a separation distance of $D = 30$ Å. Data points have been connected with a solid line in order to guide the eye.

allow for significant tunneling. The enhanced net transfer rate for shorter separation distances is due to the faster arrival of the emitted electron density to the opposite edge of the jellium. This traveling density, then, interacts with the Kohn-Sham effective potential well and, thus, is reintroduced to the near-field enhancement.

This phenomenon is depicted in Fig. 5, in which the flux as a function of z is shown for both the shortest separation distance, 20 Å, and the longest, 60 Å, at $t = 3.25$ fs. This time corresponds to the first maximum amplitude peak of the electric field for the short ramping time of $T_{\rm r} = 2.48$ fs. Both choices of $\varphi = 0$ and $\varphi = \pi$ are shown for each separation distance in order to characterize the preferential direction of the current.

For the small separation distance flux curves, ripples are present near the edges of the jellium, as opposed to the smooth nature of those of the large separation distance. This is indicative of the reflection and transmission of electron density traversing the near vacuum gap between edges and re-colliding with the jellium. In this case, more electron density is located near the jellium at any point in time and is, in turn, subject to the influence of the near-field enhancement. For the large separation distance cases, the electron density takes longer to traverse the vacuum region and is more susceptible to nearly freely following the laser and gaining energy rather than re-colliding with the jellium edges.

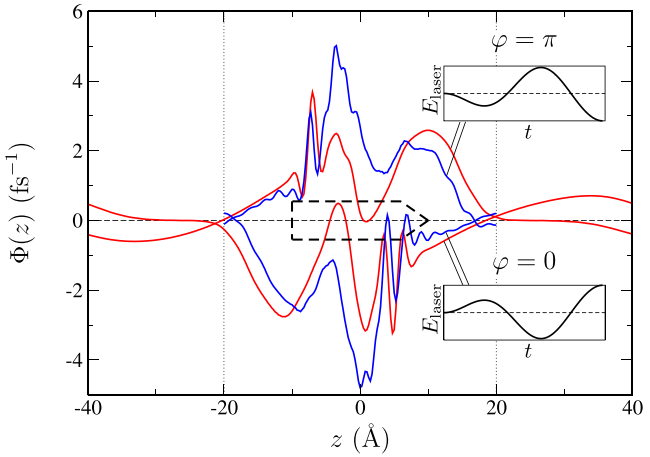

FIG. 5. Flux as a function of location along the axis of symmetry of the jellium shape, here labeled as the z-axis, at $t = 3.25$ fs. Curves dominated by positive values are related to a laser field with a phase of π while those dominated by negative values are related to a laser field with a phase of zero. Results for both the smallest separation distance of 20 Å (blue) and longest separation distance of 80 Å (red) are depicted, with vertical dotted lines at ± 20 Å indicating the box boundaries of the former case. The location of the jellium shape is outlined by the black dashed lines near the center. Insets at the top right and bottom right depict the shapes of the related laser fields as functions of time. In each simulation, parameters $I = 1.33 \times 10^{13}$ W/cm^2 and $T_{\rm r} = 2.48$ were used.

Figure 6 shows the dependence of the transfer rate on the intensity of the laser field. These simulations were similarly performed twice each in order to average results for laser phases of 0 and π. As the intensity rises, so too does the transfer rate. However, at large enough intensities, as in this case of around $I = 3 \times 10^{13}$ W/cm^2, the emission from either edge begins to become comparable and the trend in the net transfer rate, $k_{\rm tr}$, levels off.

V. CONCLUSION

In conclusion, we have computationally demonstrated laser-induced rectification by simulating the effects of increased electron emission due to near-field enhancement within a periodic jellium system with geometrical asymmetry. Such behavior opens the door for new nano-scale "vacuum-tube-based" devices which take advantage of the enhanced transport rate of electrons in vacuum, as compared to the relatively limited electron transport rates in conventional semiconductor-based devices. Our findings show a significant increase in transport rate when the distance between facing anode and cathode tips becomes small. Furthermore, we have shown an increase in the transport rate for higher laser intensities; however, for high enough laser intensities, the local near-field enhancement becomes negligible and rectification becomes less prominent.

ACKNOWLEDGMENTS

This work was supported by the National Science Foundation (NSF) under Grant Nos. OISE 1261117, PHY 1314463, and OISE 1613549.

[1]M. F. Ciappina, J. A. Prez-Hernndez, A. S. Landsman, W. A. Okell, S. Zherebtsov, B. Frg, J. Schtz, L. Seiffert, T. Fennel, T. Shaaran, T. Zimmermann, A. Chacn, R. Guichard, A. Zar, J. W. G. Tisch, J. P. Marangos, T. Witting, A. Braun, S. A. Maier, L. Roso, M. Krger, P. Hommelhoff, M. F. Kling, F. Krausz, and M. Lewenstein, Rep. Prog. Phys. **80**, 054401 (2017).
[2]B. Ahn, J. Schtz, M. Kang, W. A. Okell, S. Mitra, B. Frg, S. Zherebtsov, F. Smann, C. Burger, M. Kbel, C. Liu, A. Wirth, E. D. Fabrizio, H. Yanagisawa, D. Kim, B. Kim, and M. F. Kling, APL Photonics **2**, 036104 (2017).
[3]M. A. Gubko, W. Husinsky, A. A. Ionin, S. I. Kudryashov, S. V. Makarov, C. R. Nathala, A. A. Rudenko, L. V. Seleznev, D. V. Sinitsyn, and I. V. Treshin, Laser Phys. Lett. **11**, 065301 (2014).
[4]L. Wimmer, G. Herink, D. R. Solli, S. V. Yalunin, K. E. Echternkamp, and C. Ropers, Nat. Phys. **10**, 432 (2014).
[5]V. Schweikhard, A. Grubisic, T. A. Baker, I. Thomann, and D. J. Nesbitt, ACS Nano **5**, 3724 (2011).
[6]D. J. Park, B. Piglosiewicz, S. Schmidt, H. Kollmann, M. Mascheck, and C. Lienau, Phys. Rev. Lett. **109**, 244803 (2012).
[7]K. Yoshioka, I. Katayama, Y. Minami, M. Kitajima, S. Yoshida, H. Shigekawa, and J. Takeda, Nat Photonics **10**, 762 (2016).
[8]M. Kruger, M. Schenk, and P. Hommelhoff, Nature **475**, 78 (2011).
[9]V. Jelic, K. Iwaszczuk, P. H. Nguyen, C. Rathje, G. J. Hornig, H. M. Sharum, J. R. Hoffman, M. R. Freeman, and F. A. Hegmann, Nat. Phys. **13**, 591 (2017).
[10]T. Rybka, M. Ludwig, M. F. Schmalz, V. Knittel, D. Brida, and A. Leitenstorfer, Nat. Photonics **10**, 667 (2016).
[11]A. Schiffrin, T. Paasch-Colberg, N. Karpowicz, V. Apalkov, D. Gerster, S. Muhlbrandt, M. Korbman, J. Reichert, M. Schultze, S. Holzner, J. V. Barth, R. Kienberger, R. Ernstorfer, V. S. Yakovlev, M. I. Stockman, and F. Krausz, Nature **493**, 70 (2013).
[12]S.-G. Jeon, D. Shin, and M. S. Hur, Sci. Rep. **6**, 32567 (2016).
[13]J. Hoffrogge, J. P. Stein, M. Krger, M. Frster, J. Hammer, D. Ehberger, P. Baum, and P. Hommelhoff, J. Appl. Phys. **115**, 094506 (2014).
[14]G. Diamant, E. Halahmi, L. Kronik, J. Levy, R. Naaman, and J. Roulston, Appl. Phys. Lett. **92**, 262903 (2008).
[15]J.-W. Han, J. S. Oh, and M. Meyyappan, Appl. Phys. Lett. **100**, 213505 (2012).
[16]J.-W. Han, D.-I. Moon, and M. Meyyappan, Nano Lett. **17**, 2146 (2017).
[17]T. Higuchi, L. Maisenbacher, A. Liehl, P. Dombi, and P. Hommelhoff, Appl. Phys. Lett. **106**, 051109 (2015).
[18]K. J. Savage, M. M. Hawkeye, R. Esteban, A. G. Borisov, J. Aizpurua, and J. J. Baumberg, Nature **491**, 574 (2012).
[19]K. Yabana and G. F. Bertsch, Phys. Rev. B **54**, 4484 (1996).
[20]W. Ekardt, Phys. Rev. Lett. **52**, 1925 (1984).
[21]M. Brack, Rev. Mod. Phys. **65**, 677 (1993).
[22]M. Madjet, C. Guet, and W. R. Johnson, Phys. Rev. A **51**, 1327 (1995).
[23]J. Zuloaga, E. Prodan, and P. Nordlander, Nano Lett. **9**, 887 (2009).
[24]H. Liu, H. Wang, J. Zhao, and M. Kiguchi, J. Comput. Chem. **34**, 360 (2013).
[25]J. Hu, X. Ruan, and Y. P. Chen, Nano Lett. **9**, 2730 (2009).
[26]L. Novotny and B. Hecht, *Principles of Nano-Optics*, 2nd ed. (Cambridge University Press, 2012).
[27]N. Nakaoka, K. Tada, S. Watanabe, H. Fujita, and K. Watanabe, Phys. Rev. Lett. **86**, 540 (2001).
[28]M. Mundt and S. Kümmel, Phys. Rev. Lett. **95**, 203004 (2005).
[29]M. A. Mosquera and A. Wasserman, Mol. Phys. **112**, 2997 (2014).
[30]M. Koentopp, C. Chang, K. Burke, and R. Car, J. Phys.: Condens. Matter **20**, 083203 (2008).
[31]K. Varga and J. A. Driscoll, *Computational Nanoscience* (Cambridge University Press, England, 2011).
[32]C. Covington, D. Kidd, J. Gilmer, and K. Varga, Phys. Rev. A **95**, 013414 (2017).
[33]D. Kidd, C. Covington, Y. Li, and K. Varga, Phys. Rev. B **97**, 024303 (2018).